ELSEVIER

PII: S0032-3861(97)00425-4

Polymer Vol. 39 No. 11, pp. 2269–2280, 1998

0032-3861/98/$19.00+0.00

Reaction-induced phase separation mechanisms in modified thermosets

E. Girard-Reydet[a], H. Sautereau[a], J.P. Pascault[a,*], P. Keates[b], P. Navard[b], G. Thollet[c] and G. Vigier[c]

[a]*Laboratoire des Matériaux Macromoléculaires – UMR CNRS No. 5627, Institut National des Sciences Appliquées de Lyon, 20, Avenue A. Einstein, 69621 Villeurbanne Cedex, France*

[b]*Centre de Mise en Forme des Matériaux, Ecole des Mines de Paris – URA CNRS No. 1374, BP 207, 06904 Sophia Antipolis Cedex, France*

[c]*GEMPPM – UMR CNRS No. 5510, Institut National des Sciences Appliquées de Lyon, 20, Avenue A. Einstein, 69621 Villeurbanne Cedex, France*

(Received 25 January 1997; revised 4 April 1997)

The reaction-induced phase separation in amorphous thermoplastic–modified epoxy systems was observed *in situ* using methods of different observation windows: small angle X-ray scattering (SAXS), light transmission (LT) and light scattering (LS). The transmission electron microscopy (TEM) technique was concurrently used to get direct representations of morphologies at different levels of the phase separation process. The selected systems were bisphenol-A diglycidylether cured with either 4,4′-diaminodiphenylsulfone or 4,4′-methylenebis[3-chloro,2,6-diethylaniline] in the presence of polyetherimide. The phase separation mechanisms involved were found to be greatly dependent on the initial modifier concentration and on the ratio of the phase separation rate with respect to the polymerization rate. Experimental results showed that, for modifier concentrations close to the critical fraction, the system was directly thrown into the unstable region, even at a low polymerization rate, and phase separation proceeded by spinodal demixing. On the other hand, for off-critical compositions the homogeneous solution demixed slowly via the nucleation and growth mechanism. In spite of the evolution of the phase diagram with reaction extent, the system remains in the metastable state whatever the cure temperature. The cure temperature has a strong effect on the extent of phase separation, since sooner or later vitrification of the thermoplastic-rich phase occurs and stops the evolution of morphologies. A post-cure allows the phase separation process to go further and sub-particles can be generated depending on the precure and post-cure temperatures.

(Keywords: thermoplastic–thermoset blends; phase separation process; mechanism)

INTRODUCTION

The reaction-induced phase separation (PS) process in a rubber or thermoplastic–modified thermosetting polymer is caused by the increase in the average molar mass of the polymer superimposed by possible variations of the interaction parameter, χ with conversion[1,2]. This secondary effect may favour mixing or demixing, depending on whether χ decreases or increases, respectively, with conversion. In comparison to the use of preformed particles, the advantages of the reaction-induced PS procedure are stability and low viscosity of the initial homogeneous solution. But the most interesting fact is the possibility of generating different structures within the final material. This, however, requires an effective control of every factor involved in the PS process and an understanding of PS mechanisms.

On the basis of usual LCST or UCST phase diagrams, there are two regions of phase separation for a binary or quasi-binary system: the metastable region (i.e. the region between binodal and spinodal curves) and the unstable region where nucleation and growth (NG) and spinodal demixing (SD) are both expected to occur. The reaction-driven PS proceeds isothermally but differently from the PS in non-reactive binary blends. The quench depth, defined as the temperature difference between the LCST or UCST and the reaction temperature, increases with time. It is then usually referred to as a non-isoquench process. Recent reviews describing theoretically the PS process have been published on this subject[3,4].

Several works, mainly based on scattering studies, have been devoted to determining the PS mechanisms in such systems. Some authors gathered evidences that PS occurs by a NG mechanism when the modifier is a low molar mass reactive rubber ($\approx$ 4000 g mol^{-1}). Experimental results verifying this assessment were (i) positive diffusion coefficients, as measured *in situ* during PS[5,6] and (ii) *in situ* small angle X-ray scattering (SAXS) profiles typical of that of a random dispersion of spherical particles[7]. In addition to these experimental results, several observed experimental trends (fraction, composition and particle size distribution of dispersed domains) could be explained using equations for the PS rate derived from the NG mechanism[5,8–11]. Alternatively, SD has been found to occur based on light scattering (LS) studies for various rubber and thermoplastic additives[12–16]. The authors found both similarities and differences with respect to the isoquench SD[17].

However, an understanding of PS mechanisms requires that one can follow the process over the entire range of particle sizes. The use of a single technique, typically LS or

* To whom correspondence should be addressed

SAXS, will lead to conclusions only corresponding to a restricted observation window. Actually, the LS methods observe heterogeneous structures with sizes larger than about 1000 Å, while SAXS detects sizes larger than 20 Å. Following the phenomenon over only one of these length scales is not enough, as illustrated in the literature on the system based on diglycidylether of bisphenol-A (DGEBA) cured with 4,4′-diamino 3,3′-dimethyldicyclohexylmethane (3DCM) and in the presence of 15 wt% of reactive liquid-rubbers based on butadiene–acrylonitrile random copolymers. The LS experiment performed by Inoue on one of these systems gave scattering profiles (in[7]) similar to those obtained on other rubber–modified epoxy systems discussed in term of SD. Using SAXS on the same system, Chen *et al.*[7] found the real beginning of the PS to be earlier than the onset of PS as determined by LS, and the SAXS intensity profiles were consistent with a NG mechanism. These results are not contradictory but are rather complementary and a complete picture will be required to include both techniques. Nevertheless, assignment of a mechanism on the exclusive basis of scattering behaviour must be made with caution, and the use of a microscopy technique providing visual information about morphological changes during PS may be better able to characterize the demixing process. Okada *et al.*[18] studied the PS induced by chain-polymerization of 2-chlorostyrene in a polystyrene/dibutyl phthalate mixture followed by a time-resolved LS technique and scanning electron microscopy (SEM). It was found that, at a certain conversion, the scattered intensity started to increase rapidly while the angular dependence exhibited a maximum that was shifted to smaller angles with time. This is precisely the behaviour observed in the ordinary SD. However, observations by SEM revealed that the poly(2-chlorostyrene)-rich phase formed droplets in an early period. Coalescence and coarsening of droplets occurred later, leading to different final morphologies, depending on cure temperature.

The PS process, i.e. the trajectory followed by the reactive blend in the two-phase region of the phase diagram is determined by the ratio

$$K = \frac{\text{PS rate}}{\text{reaction rate}}$$

Verchère *et al.*[8] have speculated that low values of interfacial tensions and polymerization rates favour NG in most cases. The initial modifier concentration can also be expected to have a strong effect[19].

In this paper, the reaction-induced PS in an amorphous thermoplastic–modified epoxy system was observed *in situ* using methods with different observation windows: visible light transmission (LT), visible LS and SAXS. Morphologies were concurrently quenched at different stages of the PS process and observed by transmission electron microscopy (TEM) to get direct representations.

EXPERIMENTAL

Materials

The materials used have been already described elsewhere[20,21]. A classical diepoxy prepolymer, diglycidyl ether of bisphenol A (DGEBA), with a low polydispersity index ($\bar{n} = 0.03$) was used. Two aromatic diamines were investigated: 4,4′-diamino diphenylsulfone (DDS) and 4,4′-methylenebis [3-chloro, 2,6-diethylaniline] (MCDEA). The thermoplastic modifier was a polyetherimide (PEI) Ultem 1000 supplied by General Electric.

The chemical structures and characteristics of all reactants are listed in *Table 1*.

Formulation and cure cycle

The PEI modified mixtures were prepared in a two-step process: PEI was first dissolved at 140°C in the epoxy prepolymer, the diamine was then added at 135°C for DDS and 90°C for MCDEA. The hardeners were used at the stoichiometric ratio epoxy to amino-hydrogen groups equal to 1.

The homogeneous mixture was then precured at a selected temperature T_i. To obtain the final materials and to ensure complete networks without degradation, samples were postcured 2 h at 185°C for the MCDEA-based samples and 2 h at 215°C for the DDS-systems.

In the following, M10P denotes the system DGEBA–MCDEA with 10 wt% of PEI, and D10P denotes the system DGEBA–DDS with 10 wt% of PEI. The term 'neat' means the epoxy system without thermoplastic.

Techniques

Cloud points were determined with a light transmission device[22], a technique which begins to detect particles when average diameters are of the order of 0.1 μm. The cloud

Table 1. Characteristics of the different reactants used

Reactant	Formulæ	Supplier	$\overline{M_n}$ (g.mol^{-1})	$\overline{M_w}$ (g.mol^{-1})	Tg (°C)
4,4'-diaminodiphenylsulfone (DDS)	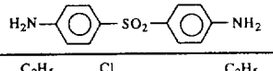	Fluka	238	/	/
4,4'-methylenebis[3-chloro 2,6-diethylaniline] (MCDEA)	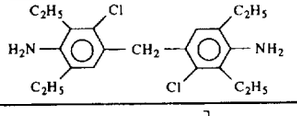	Lonza	380	/	/
diglycidyl ether of bisphenol A (DGEBA) $\bar{n}$ = 0.03	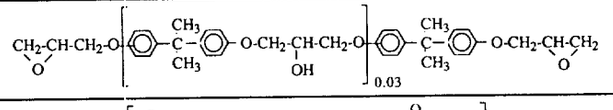	Dow Chemicals DER 332	348.5	/	/
polyetherimide (PEI)	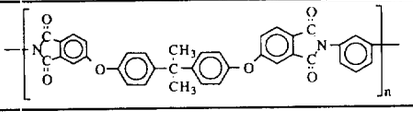	General Electric	26 000	50 000	210

point times, t_{cp}, and the cloud point temperatures, T_{cp}, were determined, respectively, as the onset times and the onset temperatures where a decrease in the transmitted light intensity was recorded. The cloud point conversions, x_{cp}, (corresponding to t_{cp}) were measured by size exclusion chromatography (SEC).

Small angle X-ray scattering was performed to follow PS at small observation scales. The scattering intensity depends on the heterogeneity of the electronic density and the size of the heterogeneous structure. The integrated intensity (I_l) of the scattered radiation was recorded as a function of the polymerization time. For a two-phase system, I_l is described as:

$$I_l \propto \Delta\rho\phi_\alpha\phi_\beta \quad (1)$$

where $\Delta\rho$ is the density difference between the two phases, and ϕ_α, ϕ_β are the volume fractions of the phases. The integrated intensity, I_l, is calculated by the following equation:

$$I_l = \int_0^\infty I(q)q^2 dq \quad (2)$$

q is the scattering vector defined as

$$q = \frac{4\pi}{\lambda}\sin\theta \quad (3)$$

where 2θ is the angle through which the radiation is scattered, and λ is the wavelength of radiation in the sample.

Depending on the investigated polymerization time, SAXS experiments were performed either on a lab set-up or on the D2–D2AM beamline at the European Synchrotron Radiation Facility (ESRF). For long polymerization times, the lab set-up was used, including a rotating anode X-ray generator with copper target and nickel filter ($\lambda = 1.54$ Å), a point collimation produced mainly by two orthogonal mirrors and a line position sensitive proportional counter connected to a computer. Samples could be heated *in situ* from room temperature up to the selected polymerization temperature, T_i. A 15 min counting time provided a good signal-to-noise ratio. The observed q values were comprised between $q_{min} = 0.01$ Å^{-1} and $q_{max} = 0.15$ Å^{-1}. Therefore, the integrated intensity was not calculated from equation (2) but in a more limited q range by

$$I_l = \int_{q_{min}}^{q_{max}} I(q)q^2 dq \quad (4)$$

This calculation made the set-up mainly sensitive to heterogeneous structures with sizes in the range 20–500 Å (for sizes lower than 20 Å or higher than 500 Å, the sensitivity is divided by a factor larger than two). Only the variations in I_l were considered, since the first recorded intensity profile (thermoplastic chains in solution in monomers) was simply substracted from each following profile. The integrated intensity determined in this way was then zero as long as the blend was homogeneous. For short polymerization times, the D2–D2AM beamline was used. Experiments were carried out in point collimation with a line position sensitive proportional counter ($\lambda = 1.36$ Å). All details of this set-up are given in[23]. Samples could be heated *in situ* from room temperature up to the selected polymerization temperature, T_i. A 60 s counting time was enough to provide very good signals. The values of q_{min} and q_{max} were 0.001 Å^{-1} and 0.05 Å^{-1}, respectively. These values made I_l mainly sensitive to heterogeneous structures with sizes in the range 60–5000 Å (for sizes lower than 600 Å or higher than 5000 Å, the sensitivity is divided by a factor larger than two). Since the intensity profiles were recorded with a very good accuracy, I_l was calculated from equation (4) by subtracting from each profile the background, taking into account the transmission coefficient of the sample. The asymptotic behaviour of the scattering intensity could be then investigated to highlight the presence or not of sharp interfaces.

Light scattering experiments were performed using unpolarized HeNe laser light ($\lambda = 632.8$ nm). Samples were mounted in a Linkam THM600 sample stage, controlled by a Linkam TMS91 temperature controller. The scattering pattern generated by the sample was visualized using a white paper screen and recorded by a standard CDD video camera. Light scattering patterns were analysed using TRAMS (time resolved analysis and measurement of scattering), an image acquisition and analysis software system from Ecole des mines, commercialized by Sematech (Nice, France). The scattered intensity function $I(q)$ was extracted from each pattern. For each profile recorded, TRAMS can extract the angular position (q_m) and intensity (I_m) of any diffuse maximum and calculate the integrated intensity (I_l).

Morphological micrographs were obtained using a JEM-200CX TEM. Ultrathin sections were prepared either at room temperature or at a lower temperature (≈ -20°C) depending on the extent of reaction of the samples. A 'natural' contrast existed between phases when a 80 kV accelerating voltage was used.

RESULTS AND DISCUSSION

Cloud point curves—kinetic studies

The cloud point curves (CPC) of the DGEBA/diamine/PEI blends prior to reaction are shown in *Figure 1*. They are typical of systems exhibiting upper critical solution temperature (UCST) behaviour. The initial miscibility is affected by the diamine: actually, the DGEBA–MCDEA system is found to be a better solvent of the PEI than the DGEBA–DDS system. However, it is worth noting the wide miscibility window available whatever the diamine is used. The theoretical composition of the thermodynamic critical point of the CPC is $\phi_{Mcrit} = 10.7$ wt% in the case of the (DGEBA–MCDEA)$_0$–PEI system and $\phi_{Mcrit} = 9.8$ wt% in

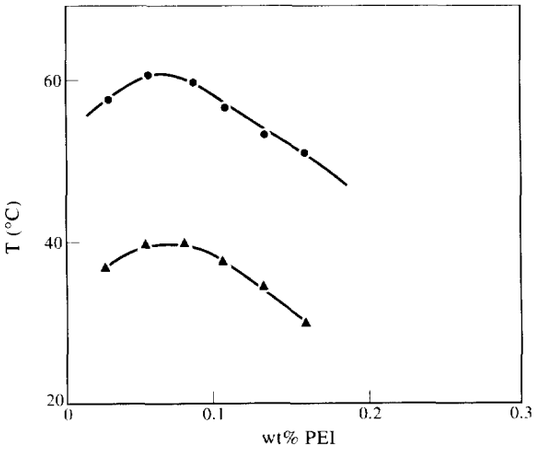

Figure 1 Initial cloud point curves for: ●, DGEBA–DDS/PEI; ▲, DGEBA–MCDEA/PEI

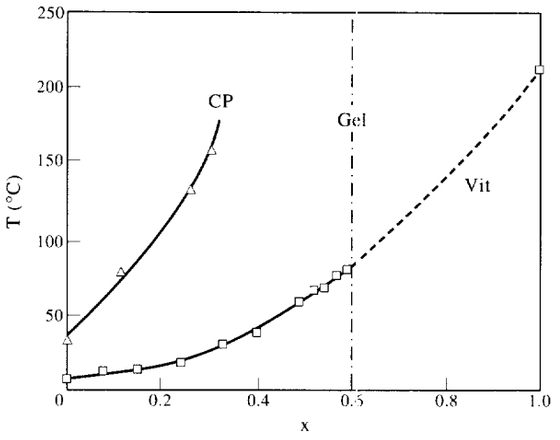

Figure 2 Experimental phase diagram temperature *versus* epoxy conversion for the M20P blend: Δ, cloud points; ◇, vitrification; – • –, gelation

the case of the (DGEBA–DDS)$_0$–PEI system, as calculated by the Flory–Huggins theory when no reaction has taken place[2]. Clarke *et al.*[24] have shown recently that the increase in ϕ_{Mcrit} during cure remained low.

The kinetic studies of these modified epoxy systems were reported elsewhere[20]. For a general discussion it is better to transform reaction times into conversions. Cloud point conversions were measured for the reactive mixtures at various PEI contents and polycondensation temperatures[2]. All of these experimental results could be plotted on the same temperature–conversion–transformation (*TxT*) diagram, as shown in *Figure 2* for the M20P system indicating phase separation at the LT scale (T_{cp}, x_{cp}), gelation (x_{gel}) and vitrification (T_g, x). The possible slight evolution of x_{gel} with composition and temperature[20] was not considered herein, and $x_{gel} = 0.60$ was assumed throughout all this study. Such diagrams are essential to control the curing of the blends with appropriate precuring and post-curing schedules.

Decomposition near the critical point

Case A: M10P, $T_i = 80°C$. Contrary to the previous study on rubber-modified epoxy[7] with similar modifier concentrations, no evolution of the scattering intensity was observed by SAXS (rotating anode). This means that no heterogeneous structure with sizes in the range 20–500 Å was generated during the PS process.

During the LS experiment, after 3200 min equivalent to t_{cp} measured by LT, a ring pattern appeared, suggesting PS was occurring. *Figure 3a* qualitatively shows the LS profiles at various stages of curing. A scattering maximum is present in each profile, indicating periodic changes in the refractive index[25] and, therefore, periodic variations in the composition of the sample. The position of the maximum can be used to estimate the characteristic repeat distance, Λ_m between regions of the same composition via the Bragg relation[26]. *Figure 3b* presents the evolution of I_m (I_m exhibits exactly the same evolution as I_1 and avoids the problems of integration boundaries) and Λ_m as a function of cure time/epoxy conversion. A time scale is also plotted to visualize better the occurring changes. Gelation and vitrification of the α phase are indicated by arrows. *Figure 4* show the morphologies observed by TEM during reaction at 80°C of the M10P blend (*a*) right after the cloud point and (*b*) after the vitrification of the α phase. The bright

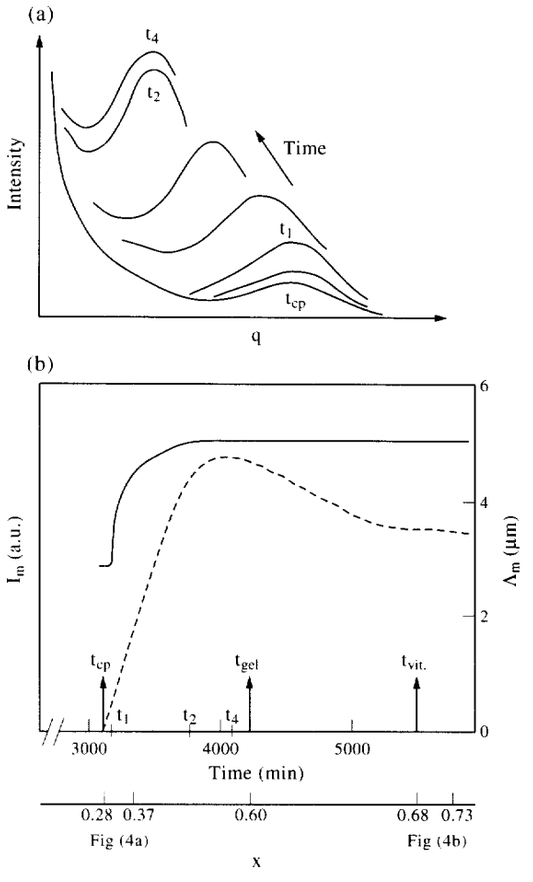

Figure 3 (a) Changes in the LS profile with curing time at $T_i = 80°C$ for the M10P system. (b) Changes in the peak intensity I_m (——) and of the periodic distance Λ_m (- - - -) with curing time/conversion at $T_i = 80°C$ for the M10P system. Cloud-point (LT), gelation and vitrification are indicated on both scales. Epoxy conversions corresponding to micrographs (*a*)–(*d*) are located on the conversion scale

domains correspond to the epoxy-rich phase and the dark ones to the PEI-rich phase.

Several observations led to the conclusion that PS was not dominated by a NG mechanism. Firstly, this mechanism would certainly cause isotropic spheres to develop at some time during the PS process. This was not observed either by SAXS or by TEM. Secondly, the variation of the scattering peak with time cannot be ascribed to the variation of a structure factor of an assembly of growing shperes[27]. On the contrary, the variation of scattering intensities and several experimental trends seem to be the hallmarks of the decomposition process of an unstable solution. The increase in peak intensity, at a constant periodic distance, between t_{cp} and t_1 may be associated to the early and intermediate stages of a SD process. In the early stage of the classical SD under isoquench (non-reactive conditions), it is accepted that periodic fluctuations in concentration, characterized by a given wavelength, develop all over the sample. This wavelength depends on the difference between the spinodal temperature and the quench depth. In the intermediate stage, the amplitude of the concentration fluctuations grows up until the equilibrium compositions are reached, but the wavelength remains constant. The demixing system is then characterized by a high level of interconnectivity in both the minor and the major phases, provided the volume fraction of the minor component is high enough. This increase in the

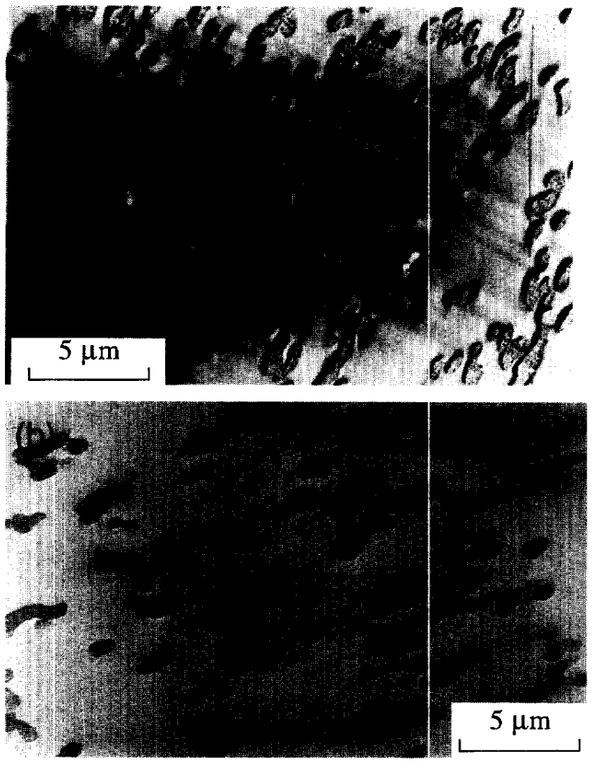

Figure 4 Transmission electron micrographs of the M10P system at different stages of PS induced by polymerization at 80°C. Corresponding epoxy conversions are (a) $x = 0.37$; (b) $x = 0.73$. The characteristics of this system are $x_{cp} = 0.28$; $x_{gel} = 0.60$ and $x_{vit\alpha} = 0.68$

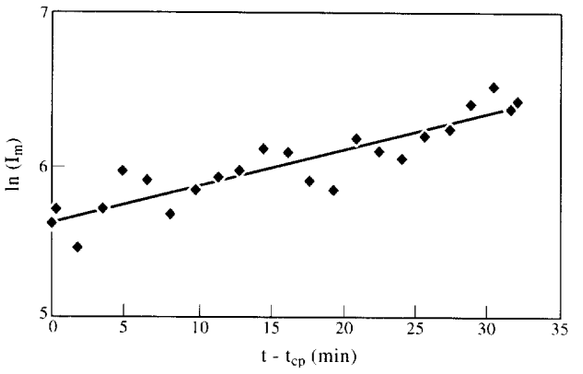

Figure 5 $\ln(I_m)$ *versus* $(t - t_{cp})$ with curing times between t_{cp} and t_1 for the M10P system at $T_i = 80°C$ (the system is assumed in iso-conversion)

peak intensity at a constant Λ_m was experimentaly observed in a short range of time ($\approx$ 20 min). Spinodal demixing is, however, known to be a rapid process in so far as the mobility is sufficient. Since the epoxy conversion increase was low between t_{cp} and t_1 (Δx lower than 0.05), it could reasonably be assumed that SD proceeded practically under isoquench during these stages. In the classical theory of SD, the linearized form of the Cahn–Hilliard diffusion equation predicts that the amplitude of fluctuation concentrations grows exponentially with time[28]. This behaviour was actually verified, as shown in *Figure 5*, exhibiting a linear dependence of $\ln(I_m)$ with the relative time $(t - t_{cp})$ for $t_{cp} \leq t \leq t_1$. After t_1, the intensity of the peak keeps on increasing monotonically but its position shifts toward smaller scattering vectors/larger periodic distances until t_2. This shift has already been observed by Yamanaka and Inoue[12] for an epoxy–DDS/19.2wt% polyethersulfone mixture. This was assigned to the coarsening process in the intermediate to last stage of the conventional thermally induced SD. The SD is, however, expected to take place under successive increases in the quench depth. Computer simulations of the time-dependent concentration fluctuation using the Cahn–Hilliard non-linear diffusion equation were performed to evaluate the demixing process under non-isoquench depth conditions[17]. It revealed that the structure coarsening may be suppressed by the increase in quench depth and that the final morphology is highly dependent on the quench rate. But in the case of low quench rate, which is actually our case, the time dependence of the LS profile is similar to that of the familiar isothermal SD and the coarsening process is definitely seen. Consequently, as the domains grow, the PEI-rich domains can no longer maintain the macroscopic percolation resulting in the formation of fragments. The fragmented domains then degenerate to minimize interfacial free energy. A decrease of phase connectivity is actually oberved when comparing TEM micrographs (*Figure 4a* and *b*).

From t_2, the periodic distance remains constant, suggesting morphology fixation. This morphology fixation may be the result of (i) a decrease in mobility due to the reaction extent (these diffusional limitations during the cure of thermosetting polymers have been modelled using an approach based on dielectric analysis[29]), and/or (ii) the vitrification of the β phase which is rich in high T_g thermoplastic. Since cure was performed at low temperature, the vitrification of the β phase is probable (but difficult to measure). A slight increase in I_m is observed until t_4, i.e. even after fixation of the geometry. Phase separation proceeds further, suggesting a further increase in the composition difference between PEI-rich and epoxy-rich regions. The decrease in I_m from t_4 is most probably caused by the variation of the refractive index between both phases[27], since polycondensation reactions still go on[30]. This is supported by the plateau starting around t_{vit}.

Case A': M10P, T_i = 160°C. To investigate the influence of the polycondensation rate, SAXS (rotating anode) and LS measurements were performed on the previous system at 160°C. Again no evolution of the scattering intensity was measured by SAXS during the whole cure. After a cure time similar to t_{cp} as measured by LT, a ring pattern of LS appeared and a peak was observed in the LS profile. The schematic evolutions of I_m and Λ_m are plotted in *Figure 6*. Once again, the combination of SAXS and LS results are the hallmarks of the decomposition process of an unstable solution similar to SD. Contrary to the experiment at 80°C, the stage where the intensity of the peak increases at a constant scattering vector is not seen any more. Since the polymerization rate is higher, the early and intermediate stages of SD may occur in a range of time too short to be visualized here. Then, from the onset of PS, the position of the peak shifts toward smaller scattering vectors. This means that, even if the cure temperature is high and probably due to the very low reactivity of the MCDEA, the quench rate remained low enough so that the coarsening process definitely occurred. Λ_m increases until t_1 and unmotivated decreases until t_2, where the maximum of I_m is reached simultaneously: morphology fixation and the end of PS occur at the same time. It can be observed that the PS

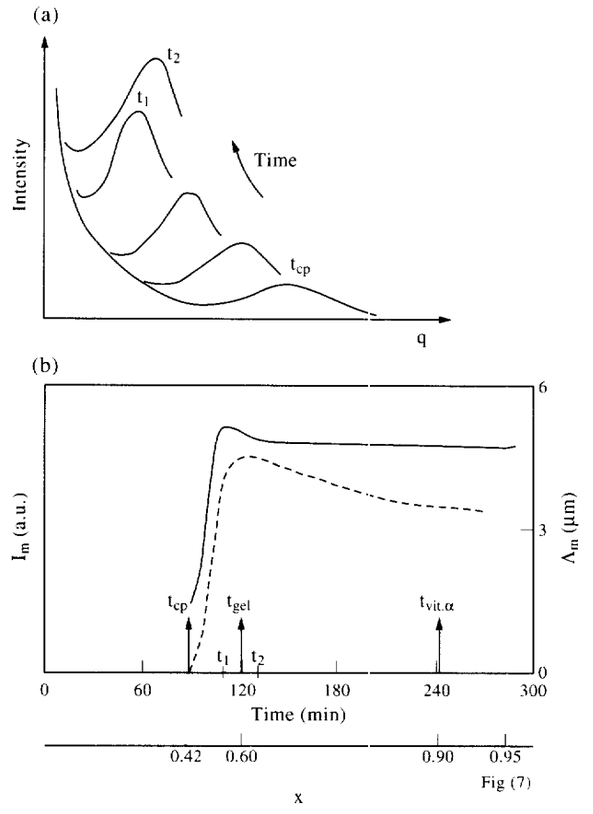

Figure 6 (a) Changes in the LS profile with curing time at $T_i = 160°C$ for the M10P system. (b) Changes in the peak intensity I_m (- - - -) and in the periodic distance Λ_m (—) with curing time/conversion at $T_i = 160°C$ for the M10P system. Cloud-point (LT), gelation and vitrification are indicated on both scales. Epoxy conversion corresponding to *Figure 7* is given on the conversion scale

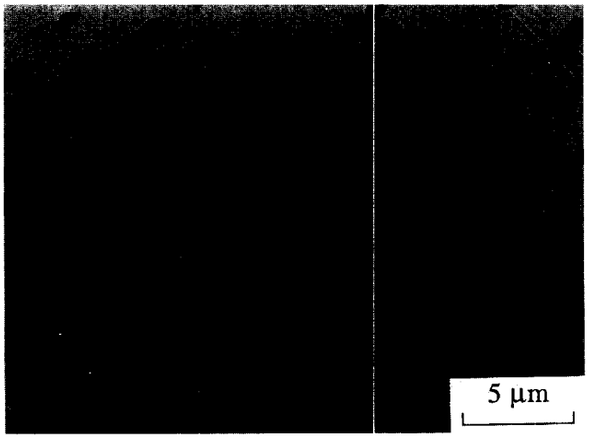

Figure 7 Transmission electron micrograph of the M10P system after vitrification of the α phase at $T_i = 160°C$ ($x = 0.95$). The characteristics of this system are $x_{cp} = 0.42$; $x_{gel} = 0.60$ and $x_{vit\alpha} = 0.90$

process is not stopped by gelation of the α phase ($t_2 > t_{gel}$). The decrease in Λ_m between t_1 and t_2 is striking. Such a decrease can have two main reasons. A change in the mean refractive index of the matrix change can slightly change the position of Λ_m, or a change in the morphology. Most probably, the second reason is the major contribution of this

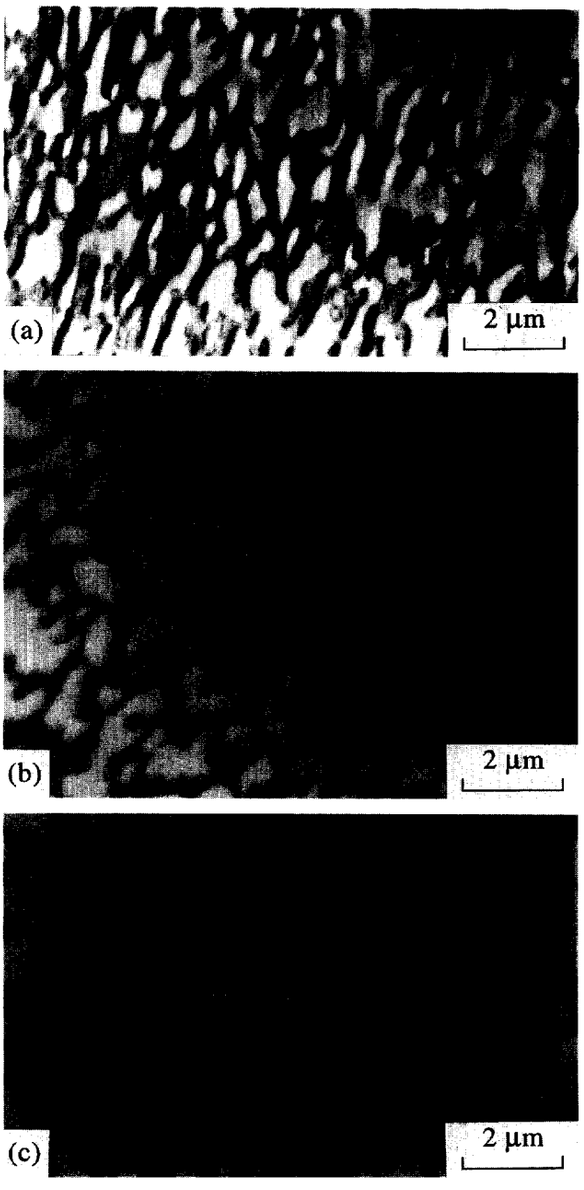

Figure 8 Transmission electron micrographs of the M20P system at different stages of PS induced by polymerization at 80°C. Corresponding epoxy conversions are (a) $x = 0.33$; (b) $x = 0.42$; (c) $x = 0.69$. The characteristics of this system are $x_{cp} = 0.26$; $x_{gel} = 0.60$ and $x_{vit\alpha} = 0.65$

change by a combination of structure break-up due to interfacial forces and multiple scattering effect linked to this breaking-up.

Figure 7 shows the morphology observed by TEM of the M10P blend after vitrification of the α phase at 160°C. The micrograph exhibits spherical PEI-rich particles (dark domains) dispersed in an epoxy-rich matrix (bright domains). At 160°C, vitrification of the β phase is a less limiting factor of the PS process than at 80°C. In addition, the viscosity at the cloud point is lower. Therefore, it is only to be expected that fragmented β domains further degenerate to minimize interfacial free energy leading to spherical particles.

Case B: M20P, T_i = 80°C. *Figure 8a–c* show the domain structures observed by TEM at different stages of the PS process after the cloud point for the M20P system at

80°C. In good agreement with the theoretical composition of the thermodynamic critical point of the CPC, phase inversion took place, leading to the formation of epoxy-rich domains dispersed within a thermoplastic-rich matrix. Micrographs (*Figure 8a* and *b*) display the development of bicontinuous structure in the early stage of PS after x_{cp}. Thereafter, the interruption of the α phase continuity proceeds and an inverted structure is finally obtained.

Scattering experiments were not realized on this system. However, the evolution of morphologies at 80°C, as revealed by TEM, shows obviously that SD was involved as well.

Decomposition for off-critical composition

Case C: M30P, T_i = **100°C.** The curing temperature, 100°C, was choosen low with respect to the diamine reactivity. The cloud point time was first determined using LT. A slight decrease in the transmitted light was measured after a cure time $t_{cp} = 1100$ min. Light scattering measurements showed the appearance of some scattering at t_{cp}, but the intensity remained to low and no scattering profile could be extracted from the noisy signal. After a cure time $t_1 = 650$ min (well before t_{cp}), an increase in the scattering intensity was measured by SAXS (rotating anode), suggesting

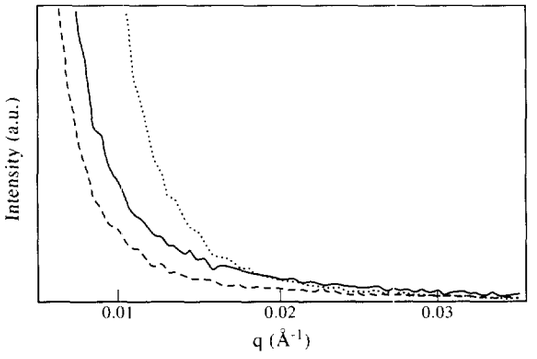

Figure 9 Changes in the SAXS profile with curing time common to case C and C'. The presented curves correspond to the M30P system cured at 160°C (case C'). Corresponding times are : - - - -, t = 60 min; —, t = 110 min; ....., t = 150 min

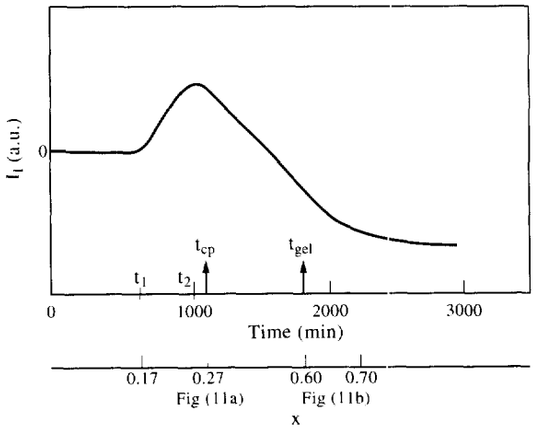

Figure 10 Changes in the integrated intensity I (arbitrary unit) with curing time/epoxy conversion at T_i = 100°C for the M30P system. Cloud-point (LT) and gelation are indicated on both scales. Epoxy conversions corresponding to *Figure 11a* and *b* are given on the conversion scale

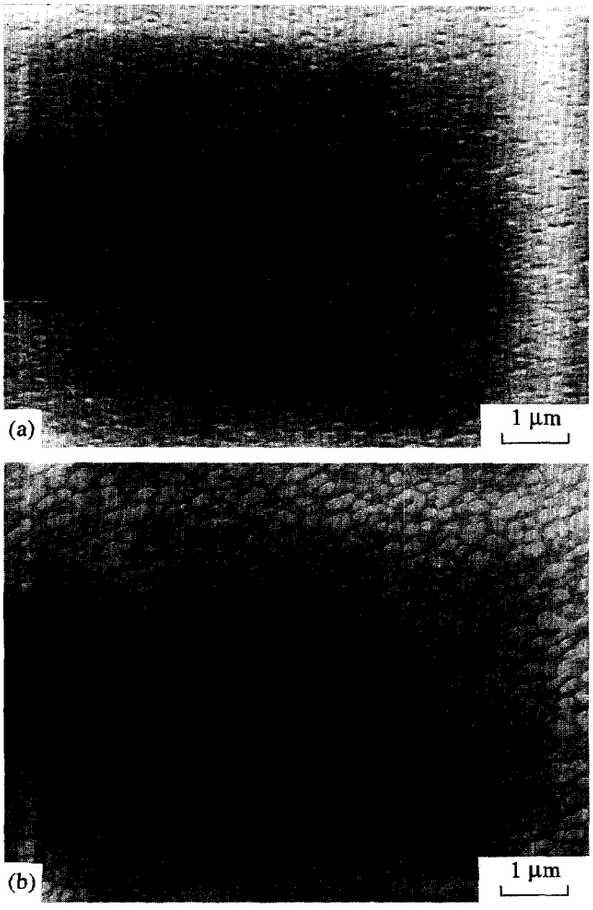

Figure 11 Transmission electron micrographs of the M30P system at different stages of PS induced by polymerization at 100°C. Corresponding epoxy conversions are (a) $x = x_{cp} = 0.27$; (b) $x = 0.70$. The characteristics of this system are $x_{cp} = 0.27$; $x_{gel} = 0.60$

that a heterogeneous structure was appearing in the SAXS window. *Figure 9* (common to case C') shows typical changes of the scattering intensity at different cure times. No maximum was observed on the scattering profiles. The integrated intensity, I_1 was plotted *versus* cure time and epoxy conversion in *Figure 10*. Cloud point, gelation and vitrification times are indicated by arrows. *Figure 11* show the morphologies observed by TEM of the M30P blend, (*a*) right after the cloud point and (*b*) after the vitrification of the α phase. Resulting conversions are located on the conversion scale of *Figure 10*. The monotonically decreasing scattering profiles with q, the I_1 curve and TEM observations are characteristic of the decomposition process of a metastable solution.

The I_1 curve can be divided into three zones: zone 1 (until t_1), zone 2 (from t_1 to $t_2 = 1000$ min) and zone 3 (after t_2). The solution, homogeneous in zone 1, started to demix at t_1, where some changes in the scattering intensity were recorded. It can be seen that a precipitated phase appeared much earlier than the cloud point time. Before t_{cp}, the size of the precipitated particles is always smaller than 1000 Å, since LT and LS techniques cannot detect it. I_1 monotonically increased in zone 2 corresponding to the nucleation/growth of α (epoxy-rich) particles in the SAXS window. The decrease in zone 2 could be attributed to the variation in phase size. Because the size of some particles

became greater than that of the SAXS window (≈ 500 Å), the increase in scattering by newly appearing particles or by the growth of smaller particles could not compensate for this disappearance of large particles. Since a cloud point was seen by LT, the PS proceeded further so that some particles reached sizes around 1000 Å. This is clearly supported by *Figure 11a* which exhibits epoxy-rich particles with sizes ranging from around 500 Å to 1000 Å dispersed in a PEI-rich matrix. The quasi-spherical shape of these α particles (if one takes into account their inescapable deformation during preparation of ultrathin sections due to the low T_g, corresponding to the low epoxy conversion) is an additional argument for the NG mechanism.

Figure 11b shows that epoxy-rich particles kept on growing after t_{cp} but their sizes at the end of the PS process remained low (≈ 2000 Å). This can justify the very low LS intensity recorded. Owing to the low cure temperature, the vitrification of the β phase probably fixes the size of particles in the beginning of the LS window. Additionally, the high viscosity of this system with 30 wt% of modifier reduces the phase separation rate.

Case C': M30P, T_i = 160°C. Small angle X-ray scattering (synchrotron radiation source) was performed on the M30P blend at 160°C. Curves of scattering intensity *versus* q at different cure times are like those in *Figure 9*: no maximum was observed on the scattering profiles. The integrated intensity, I_I was plotted *versus* cure time and epoxy conversion in *Figure 12*. Cloud point (determined by LT) and gelation times are indicated by arrows.

The I_I curve can be once again divided into three zones: zone 1 (until t_1 = 70 min), zone 2 (from t_1 to t_2 = 110 min) and zone 3 (after t_2). A non-zero constant scattering intensity was measured for cure times lower than t_1, exhibiting an asymptotic q^{-1} behaviour for large q. This feature is characteristic of the scattering function of persistence chains[31]. Scattering in zone 1 then corresponds to the scattering of rigid thermoplastic chains in solution with the growing epoxy–amine copolymer. From t_1, the onset time of PS, the evolution of I_I was similar to that observed in case C. I_I monotonically increased in zone 2, corresponding to the nucleation/growth of α particles in the SAXS window. After t_2, the disappearence of the large

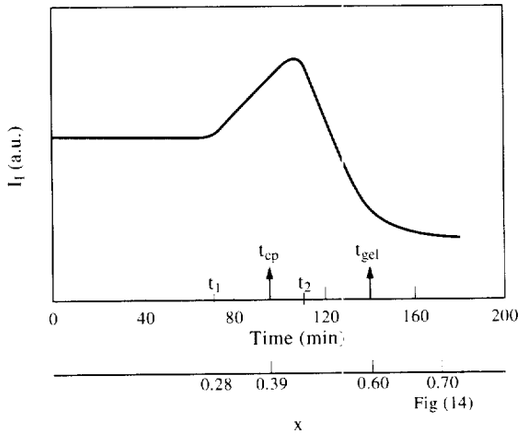

Figure 12 Changes in the integrated intensity I_I (arbitrary unit) with curing time/epoxy conversion at T_i = 160°C for the M30P system. Cloud-point (LT) and gelation are indicated on both scales. Epoxy conversion corresponding to *Figure 14* is given on the conversion scale

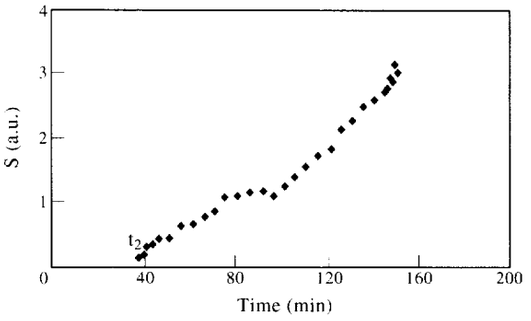

Figure 13 Evolution of the total interface of α phase, S with curing time for the M30P system at 160°C

particles of the observation window could not compensate for the increase in scattering by possible newly appearing particles or/and the growth of smaller particles, and I_I consequently decreased. t_2 was larger than t_{cp} = 95 min, since larger particles (lower q) could be observed with this technique. No particular change in the scattering profiles, which would indicate a sudden instability of the demixing solution, was observed. This means that, in spite of the evolution of the phase diagram with reaction extent and the higher reactivity of the system, the solution remains in the metastable state during the whole PS process.

However, the NG mechanism implies that the interface between the phases is sharp. An asymptotic behaviour of the scattering intensity was then expected, where the fourth power Porod's law is valid, i.e.

$$\lim I(q)_{q\to\infty} \propto \frac{S}{q^4} \tag{5}$$

where S is the total interface. When plotting ln $I(q)$ *versus* ln q for large q, the -4 slope was actually obtained only for cure times longer than around 110 min. Alternatively, all $I(q, t)$ curves could be modelled using the sole following asymptotic equation:

$$\lim I(q,t)_{q\to\infty} \propto \frac{S(t)}{q^4} + \frac{B(t)}{q} \tag{6}$$

This asymptotic behaviour characterizes the additional scattering of demixing particles via the NG mechanism to scattering of persistence chains still in solution. Equation (6) corresponds to a straight line in a plot of $q\,I(q, t)$ *versus* q^{-3} for large q, the slope of which allows the determination of $S(t)$ and the ordinate at the origin which allows the determination of $B(t)$. $B(t)$ contains information on chain properties. It is, however, not directly related to the PS process. For the sake of clarity, $B(t)$ and its possible correlation with $S(t)$ will be discussed elsewhere[32]. Only general trends are considered here: $B(t)$ remained constant until t_1 and tended towards zero for large t, where Porod's law becomes valid. The evolution of S with time is presented in *Figure 13*. $S(t)$ was zero as long as the solution remained homogeneous. Thereafter, $S(t)$ monotonically increased from the onset until the end of the PS process, meaning that the total interface continually increased. Hence, the latest stage of demixing was not dominated by the coalescence of particles. The high viscosity of this system may be the reason. The morphology obtained after gelation is shown in *Figure 14*. α particles were larger than those observed in *Figure 11b* (same conversion), since vitrification of the thermoplastic-rich occurred later at 160°C.

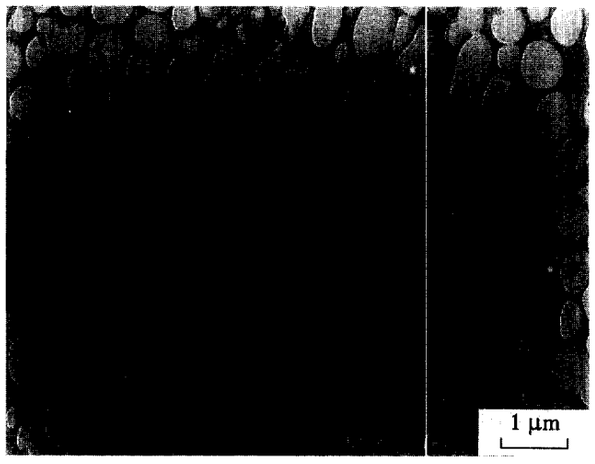

Figure 14 Transmission electron micrographs of the M30P system after gelation of the a phase at $T_i = 160°C$ ($x = 0.70$). The characteristics of this system are $x_{cp} = 0.39$; $x_{gel} = 0.60$

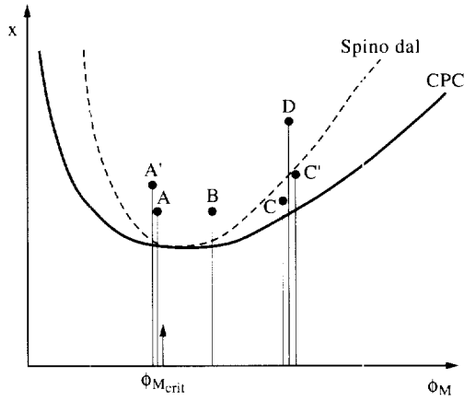

Figure 15 Phase diagram conversion *versus* modifier concentration: —, cloud point curve; - - - -, spinodal curve. ϕ_{Mcrit} denotes the critical modifier concentration

Discussion on the PS mechanisms

Figure 15 shows a scheme describing a conversion *versus* ϕ_M phase diagram that indicates the location of cloud point and spinodal curves. Theoretically, the solution, homogeneous at conversion below the CPC, becomes metastable between the two curves and unstable above the spinodal curve. The CPC is tangent to the spinodal curve at ϕ_{Mcrit}. The existence of a uniquely defined spinodal line is still an open question. Therefore, in practice, one should better retain the idea that the further within the two-phase region, the less stable the homogeneous solution and the more rapid its decomposition are. This is emphasized when the initial modifier concentration is much lower or much higher than ϕ_{Mcrit}. The four experimental cases studied through TEM observations and *in situ* scattering experiments are schematically reported on this phase diagram. They represent a combination of the two most important factors affecting the PS process: (i) the modifier concentration as compared with ϕ_{Mcrit}; (ii) the K value expressing the competition between PS and polymerization rates.

(a) For modifier concentrations ϕ_M close to ϕ_{Mcrit} (cases A, A' and B), the system is directly thrown into the unstable region and PS proceeds by SD, even if the polymerization rate is very low ($K \rightarrow \infty$). Due to very low reactivity of the DGEBA–MCDEA system, SD under non-isoquench conditions was found to be very similar to the classical isoquench SD whatever the cure temperature. The cure temperature only affects the extent of PS by fixing the viscosity at the cloud point and the vitrification time of the thermoplastic-rich phase. The higher T_i, the further the coarsening process goes and the more dispersed domains can minimize the interfacial free energy.

(b) For modifier concentrations much higher than ϕ_{Mcrit} (cases C and C'), the homogeneous solution enters into the metastable region and PS proceeds slowly via the NG mechanism. In spite of the evolution of the phase diagram with reaction extent, the system remains in the metastable state whatever the cure temperature. The cure temperature affects the extent of PS as well: the higher T_i, the further the growth of particles goes. Owing to the increase of the viscosity and the vitrification of the PEI-rich phase, the latest stage of demixing was not dominated by the coalescence of particles.

(c) One can imagine that, for such off-critical compositions, a very fast polymerization rate compared with the PS rate ($K \rightarrow 0$) could throw the system far enough into the two-phase region so that it would become unstable (hypothetical case D). This situation is, however, unlikely to occur with such a low reactive DGEBA–MCDEA system, even for a high cure temperature. The use of very reactive systems may be more favourable. Anyway, if we consider the possibility of a metastable → unstable evolution, the demixing process could not follow a NG law anymore, but it could not follow a classical SD law as well, since particles pre-exist. One may, therefore, think about what happens as particles corresponding to preferential wavelengths of the SD process are preferentially developed. Such a scenario may explain SAXS and LS results obtained in our previous experiments on a rubber–modified epoxy system (described in the Introduction).

Discussion on the influence of the hardener and of post-cure on final morphologies

Figures 16 and 17 give the evolution of morphologies presented on *Figure 4b* (M10P) and *Figure 8c* (M20P) after a post-cure of 2 h at 185°C. The post-cure temperature was choosen slightly higher than $T_{g\infty} = 177°C$ of the neat system to ensure a complete network without any degradation. Note that the post-cure temperature remains lower than $T_g = 210°C$ of the PEI. To investigate the influence of the relative position of the post-cure temperature *versus* T_g of the PEI, the evolution of the morphologies were also followed for PEI–modified DGEBA–DDS systems. Indeed, $T_{g\infty} = 214°C$ of the DGEBA–DDS matrix is higher than T_g of the PEI. *Figure 18a* and *Figure 19a* show the morphologies of the D10P and D20P blends after vitrification of the epoxy-rich phase at a precure temperature of $T_i = 80°C$. *Figure 18b* and *Figure 19b* present the morphologies of the same samples post-cured 2 h at 215°C.

If we first consider systems exhibiting phase inversion (M20P and D20P), it appears that the post-cure allowed devitrification of both α and β phases and, due to the extent of the reactions, PS proceeded further involving mass transfers. Therefore, ϕ_β decreases and the size of the α domains increased. For the M20P system, 185°C was high enough to confer mobility to the β phase, since a significant amount of epoxy was found to remain trapped therein.

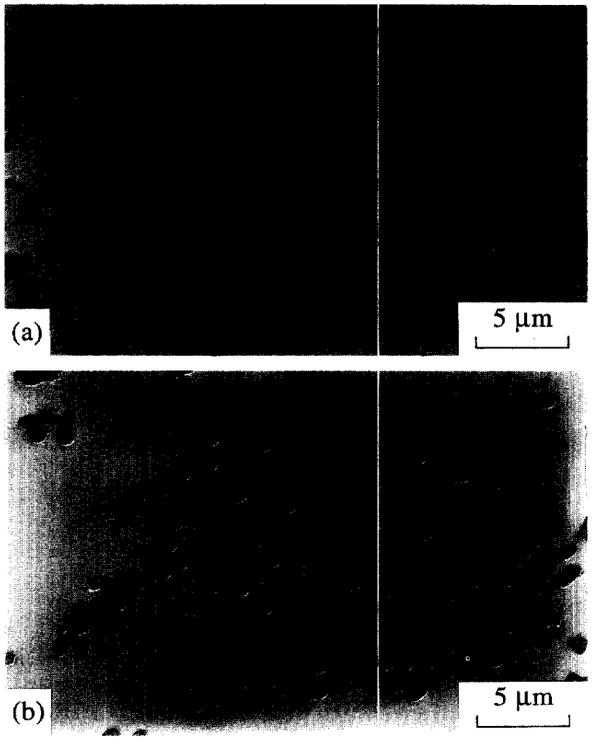

Figure 16 Transmission electron micrographs of the M10P system. (a) x = 0.72 during precure at T_i = 80°C; (b) post-cured 2 h at 185°C ($x \rightarrow 1$)

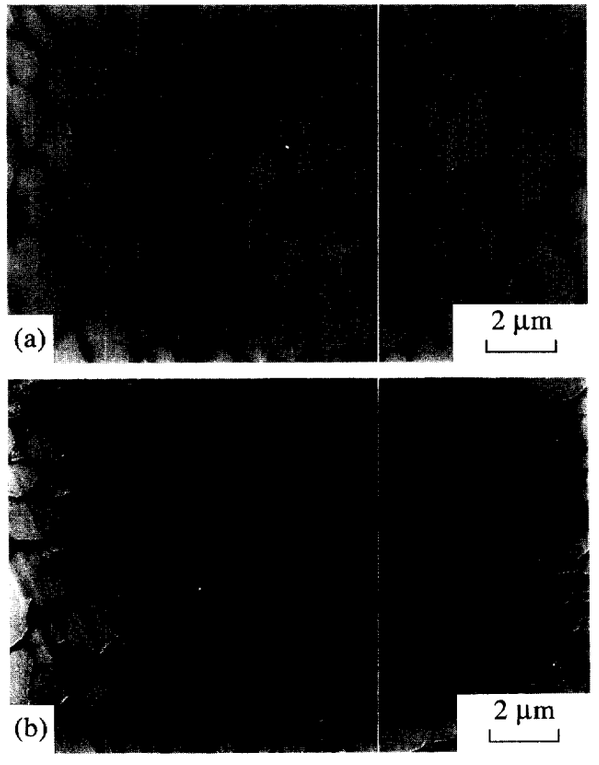

Figure 17 Transmission electron micrographs of the M20P system. (a) x = 0.69 during precure at T_i = 80°C; (b) post-cured 2 h at 185°C ($x \rightarrow 1$)

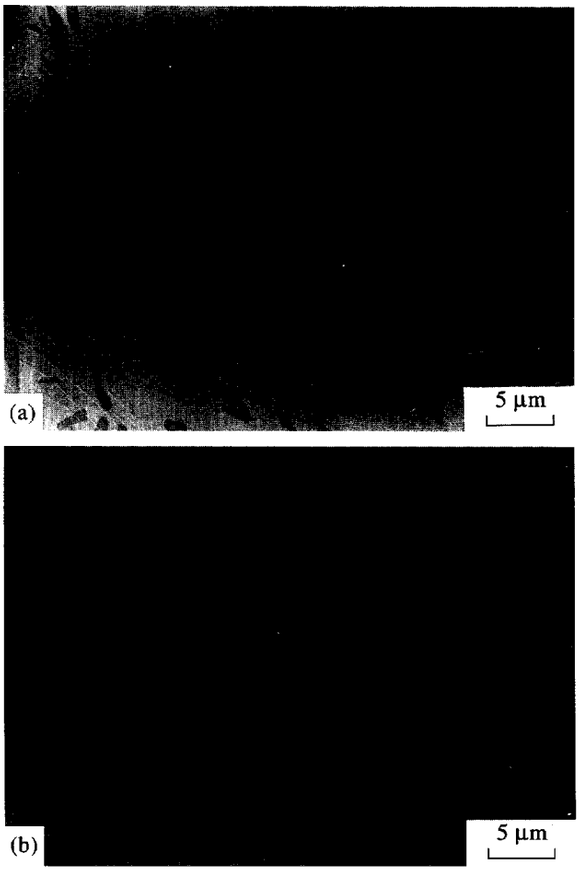

Figure 18 Transmission electron micrographs of the D10P system. (a) x = 0.62 during precure at T_i = 80°C; (b) post-cured 2 h at 185°C ($x \rightarrow 1$)

For systems modified with 10 wt% of PEI, the situation is somewhat different. In the case of D10P, it can be seen that bright sub-particles developed in the PEI-rich domains after post-cure. Sulfur microanalysis highlighted that these sub-particles consisted in epoxy small domains. For the M10P blend, given the quality of the TEM image, one can speculate on the extent to which variations within the PEI-rich particles exist. For these systems, vitrification of the β phase during precure also trapped some low polymerized epoxy–amine species (probably in lower proportion than with 20 wt%). During post-cure, reactions go further and a new driving force for unmixing exists within the PEI-rich domains. When post-cure was performed at 215°C, mobility in the β phase became high enough so that sub-particles could be formed. On the contrary, mobility at 185°C remained probably too low and no evolution of the structure inside the particles was clearly seen.

CONCLUSION

The reaction-induced phase separation in an amorphous thermoplastic–modified epoxy system was observed *in situ* with the help of different techniques with different observation windows. Depending on the initial modifier concentration, two decomposition processes were highlighted.

For modifier concentrations close to the critical composition, ϕ_{Mcrit}, the system is directly thrown into the unstable region and PS proceeds by SD. Due to very low reactivity of the DGEBA–MCDEA system, SD under non-isoquench

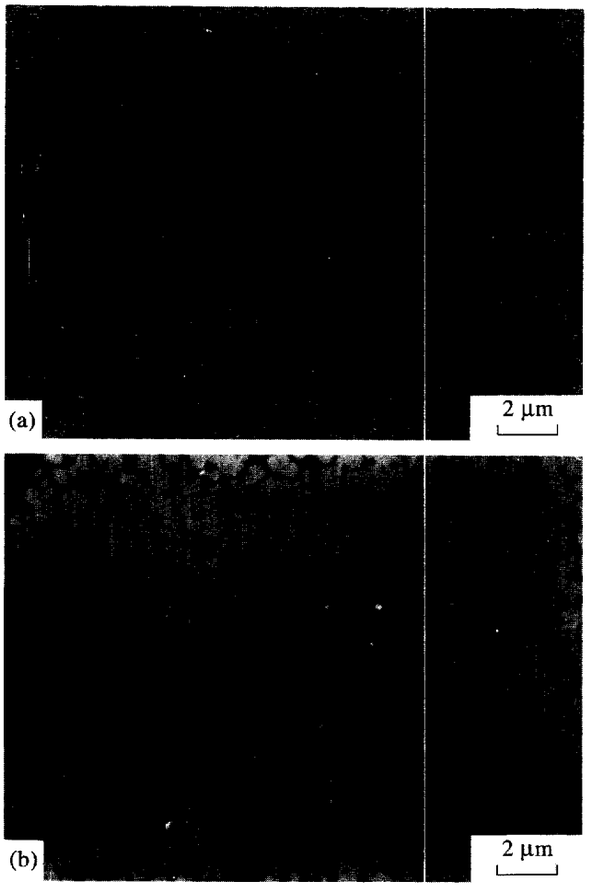

Figure 19 Transmission electron micrographs of the D20P system. (a) $x = 0.59$ during precure at $T_1 = 80°C$; (b) post-cured 2 h at 185°C ($x \rightarrow 1$)

conditions was found to be very similar to the classical isoquench SD, whatever the cure temperature. In the case of a low cure temperature, the early stage of the classical SD was even observed.

For modifier concentrations much higher than ϕ_{Mcrit}, the homogeneous solution enters into the metastable region and PS proceeds slowly via the NG mechanism. In spite of the evolution of the phase diagram with reaction extent, the system remains in the metastable state whatever the cure temperature. In both cases, the cure temperature only affects the extent of PS by fixing the viscosity at the cloud point and the vitrification time of the thermoplastic-rich phase.

For off-critical compositions, one can expect that a very fast polymerization rate compared with the PS rate could lead to a metastable → unstable evolution of the demixing solution. The demixing process could then not follow a NG law anymore but it could not follow a classical SD law either, since particles pre-exist. One may, therefore, think about what happens as particles corresponding to preferential wavelengths of the SD process are preferentially developed. This situation is, however, unlikely to occur with such a low reactive DGEBA–MCDEA system even for a high cure temperature. Alternatively, cyanates[33] which are easily catalysable may be an appropriate thermoset system to test this assumption.

During post-cure, the decomposition process can go on since (i) the post-cure allows devitrification of both phases, (ii) epoxy–amine reactions go further and a new driving force for unmixing is therefore generated in both phases. Nevertheless, the final morphologies remain greatly determined by the precure stage.

ACKNOWLEDGEMENTS

The authors wish to thank (i) the Centre de Miscoscopie Electronique Appliquée à la Biologie et à la Géologie (CMEABG) and especially Isabelle Bornard for preparing ultrathin sections; (ii) the European Synchrotron Radiation Facility (ESRF) and D2–D2AM Collaborating Research Groups (CRG); (iii) the Direction Recherche Etudes et Techniques (DRET) for financial support.

REFERENCES

1. Borrajo, J., Riccardi, C. C., Williams, R. J. J., Cao, Z. Q. and Pascault, J. P., *Polymer*, 1995, **36**, 3541.
2. Riccardi, C. C., Borrajo, J., Williams, R. J. J., Girard-Reydet, E., Sautereau, H. and Pascault, J. P., *J. Polym. Sci., Part B*, 1996, **34**, 349.
3. Williams, R. J. J., Rozenberg, B. A. and Pascault, J. P., *Advances in Polymer Science*, 1996, **128**, 95.
4. Inoue, T., *Prog. Polym. Sci.*, 1995, **20**, 119.
5. Volkov, V. P., Roginskaya, G. F., Chalykh, A. E. and Rozenberg, B. A., *Usp Khim.*, 1982, **51**, 1733.
6. Roginskaya, G. F., Volkov, V. P., Chalykh, A. E., Matveev, V. V., Rozenberg, B. A. and Enikolopyan, N. S., *Dokl. Akad. Nauk. USSR*, 1980, **252**, 402.
7. Chen, D., Pascault, J. P., Sautereau, H. and Vigier, G., *Polym. Int.*, 1993, **32**, 369.
8. Verchère, D., Sautereau, H., Pascault, J.P., Moschiar, S. M., Riccardi, C. C. and Williams, R. J. J., in *Toughened Plastics I: Science and Engineering*, ed. C. K. Riew and A. J. Kinloch. *Adv. Chem. Ser.*, 1993, Vol. 233, p. 335.
9. Williams, R. J. J., Borrajo, J., Adabbo, H. E. and Rojas, A. J., in *Rubber–Modified Thermoset Resins*, ed. C. K. Riew and A. J. Kinloch. *Adv. Chem. Ser.*, 1984, Vol. 208, p. 195.
10. Vazquez, A., Rojas, A. J., Adabbo, H. E., Borrajo, J. and Williams, R. J. J., *Polymer*, 1987, **28**, 1156.
11. Rozenberg, B. A., *Macromol. Chem., Makromol. Symp.*, 1991, **41**, 165.
12. Yamanaka, K. and Inoue, T., *Polymer*, 1989, **30**, 662.
13. Yamanaka, K., Takagi, Y. and Inoue, T., *Polymer*, 1989, **30**, 1839.
14. Yamanaka, K. and Inoue, T., *J. Mater. Sci.*, 1990, **25**, 241.
15. Hsich, H. S. Y., *J. Mater. Sci.*, 1990, **25**, 1568.
16. Hsich, H. S. Y., *Polym. Eng. Sci.*, 1990, **30**, 493.
17. Ohnaga, T., Chen, W. and Inoue, T., *Polymer*, 1994, **35**, 3774.
18. Okada, M., Fujimoto, K. and Nose, T., *Macromolecules*, 1995, **28**, 1795.
19. Jo, W. H. and Ko, M. B., *Macromolecules*, 1994, **27**, 7815.
20. Girard-Reydet, E., Riccardi, C. C., Sautereau, H. and Pascault, J. P., *Macromolecules*, 1995, **28**, 7608.
21. Girard-Reydet, E., Riccardi, C. C., Sautereau, H. and Pascault, J. P., *Macromolecules*, 1995, **28**, 7599.
22. Verchère, D., Sautereau, H. , Pascault, J.P., Moschiar, S. M., Riccardi, C. C. and Williams, R. J. J., *Polymer*, 1989, **30**, 107.
23. Roth, M., Ferrer, J. L., Berar, J. F. and Simon, J. P., in *ESRF, Beamline Handbook*, 1995, p. 41.
24. Clarke, N., McLeish, T. C. B. and Jenkins, S. D., *Macromolecules*, 1995, **28**, 4650.
25. Wickramasinghe, N. L., *Light Scattering Functions of Small Particles*. John Wiley, New York, 1973.
26. Fujita, H., in *Studies in Polymer Science*. Elsevier, Amsterdam, Chap. 9, 1990.
27. Maugey, J., Ph.D. thesis, work in progress.
28. Martin, G., *Solid State Phase Transformations in Metals and Alloys*. Ecole d'été d'Aussois, Editions de Physique, Orsay, 1978, p. 374.
29. Deng, Y. and Martin, G. C., *Macromolecules*, 1994, **27**, 5141.
30. Kim, B. S., Chiba, T. and Inoue, T., *Polymer*, 1995, **36**, 67.
31. Kirste, R. G., Oberthur, R. C., in *Small Angle X-Ray Scattering*, ed. O. Glatter and O. Kratky. Academic Press, London, 1982, p. 407.
32. Girard-Reydet, E., Pascault, J. P., David, L. and Vigier, G., to be submitted.
33. Cao, Z. Q., Mechin, F.and Pascault, J. P., in *Toughened Plastics I: Novel approaches in Science and Engineering*, ed. C. K. Riew and A. J. Kinloch. *Adv. Chem. Ser. ACS*, Vol. 252, 1996, p. 177.